

EM Implosion Memos

Memo 43

May, 2010

**150 Ω impedance-matched bicone switch configuration
with a spherical pressure vessel**

Prashanth Kumar, Serhat Altunc, Carl E. Baum, Christos G. Christodoulou and Edl Schamiloglu

University of New Mexico

Department of Electrical and Computer Engineering

Albuquerque, NM 87131

Abstract

In this paper, numerical simulations are used to investigate the 150 Ω impedance-matched bicone switch configuration with a spherical pressure vessel. The near-field electric field responses and the focal impulse waveforms are compared for cylindrical and spherical hydrogen chamber geometries.

1 Introduction

Analogous to [1], this paper compares cylindrical and spherical hydrogen chambers with a spherical pressure vessel for a 150Ω impedance-matched (IM) vertical bicone switch configuration. The switch system components, i.e., hydrogen chamber and pressure vessel, and the surrounding oil medium are identical to those in [1].

2 Setup

The VBCS-75¹ configuration in [2] is modified in this paper to maintain a fixed impedance in the pressure vessel and oil media. As seen below, this is accomplished using two bicones. A cylindrical support section (CSS) between the two cones provides structural support to the pressure vessel.

2.1 Structure visualization

2.1.1 VBCS-IM-75-SPVCHC

Figure 2.1 shows the perspective view of the VBCS-IM-75 with the spherical pressure vessel and cylindrical hydrogen chamber (SPVCHC) and the reflector. The details of the switch geometry are shown in Fig. 2.2. All components are centered at the first focal point.

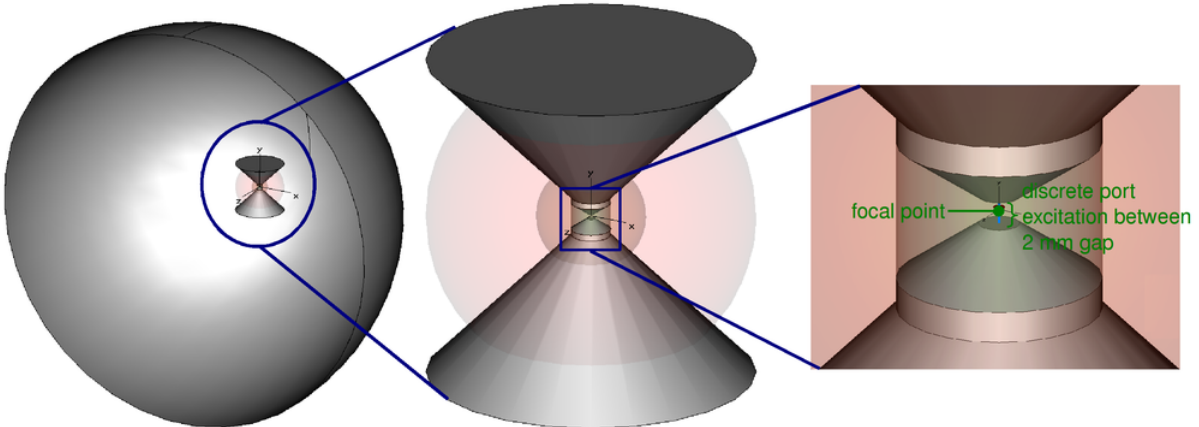


Figure 2.1: Perspective view of VBCS-IM-75-SPVCHC configuration with reflector; “Zoomed-in” view showing discrete port excitation.

The excitation is applied between bicone-1 while bicone-2 is used to guide the spherical waves originating from the source. As shown in Fig. 2.2, a cylindrical support structure, of height H_{CSS} , is used to transition between the bicones.

Bicone-1 has an impedance of 150Ω in the pressure vessel medium, i.e.,

$$\theta_1 = 2 \operatorname{arccot} \left(\exp \left[2\pi \frac{Z_c}{\sqrt{\epsilon_{r_{\text{pv}}}}} \sqrt{\frac{\epsilon_0}{\mu_0}} \right] \right) = 55.12^\circ. \quad (2.1)$$

¹Recall from [2] that the notation VBCS- Z_c refers to a vertical bicone switch with impedance $2Z_c \Omega$

Bicone-2 an impedance of 150Ω inside the oil medium, i.e.,

$$\theta_2 = 2 \operatorname{arccot} \left(\exp \left[2\pi \frac{Z_c}{\sqrt{\epsilon_{r_{oil}}}} \sqrt{\frac{\epsilon_0}{\mu_0}} \right] \right) = 46.96^\circ. \quad (2.2)$$

Hence, the impedance of the bicones remains fixed as the wave propagates from the pressure vessel into the surrounding oil medium. This is advantageous as it reduces the reflections.

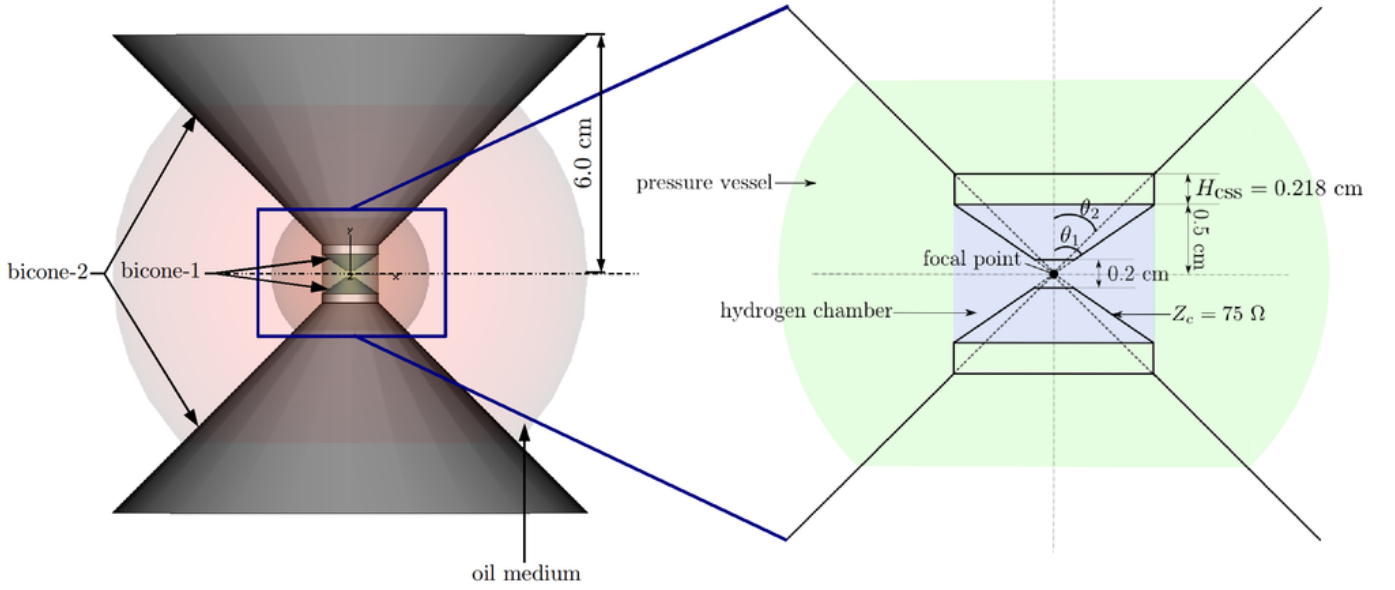


Figure 2.2: Geometrical details and “zoomed-in” side view of switch system for the VBCS-IM-75-SPVCHC configuration.

The physical dimensions of the switch system components are summarized in Table 1.

Component	Height (cm)	Radius (cm)
(mono)cone-1	$h_1 = 0.5$	$r_1 = h_1 \tan \theta_1$
cylindrical support	$H_{css} = 0.218$	$r_{css} = h_1 \tan \theta_1$
(mono)cone-2	$h_2 = 6.0$	$r_2 = h_2 \tan \theta_2$
hydrogen chamber	$h_{hc} = 1.0$	$r_{hc} = h_{hc} \tan \theta_1$
pressure vessel	–	$r_{pv} = 2.0$
oil medium	–	$r_{oil} = 6.0$

2.1.2 VBCS-IM-75-SPVSHC

Figure 2.3 shows the perspective view of the VBCS-IM-75 with the spherical pressure vessel and spherical hydrogen chamber (SPVSHC) and the reflector. The details of the switch geometry are shown in Fig. 2.4.

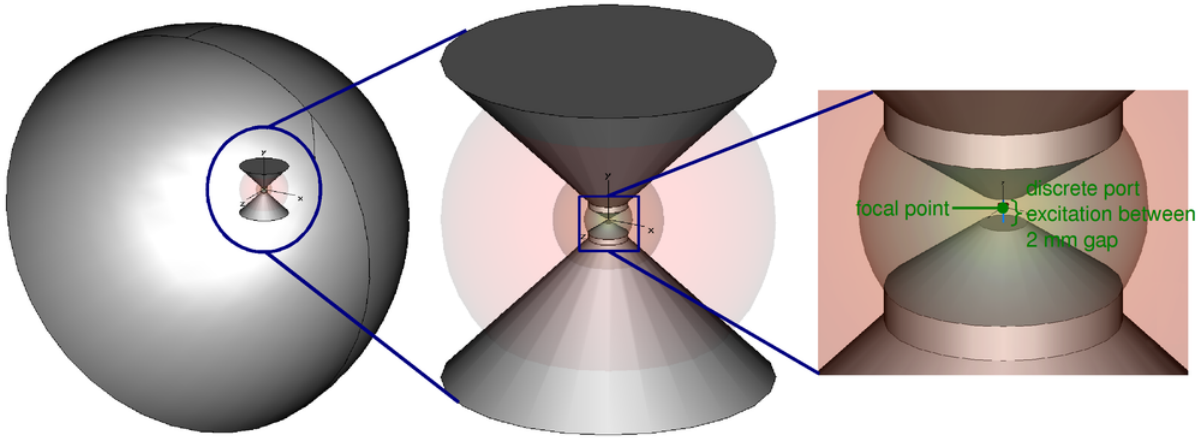


Figure 2.3: Perspective view of VBCS-IM-75-SPVSHC configuration with reflector; “Zoomed-in” view showing discrete port excitation.

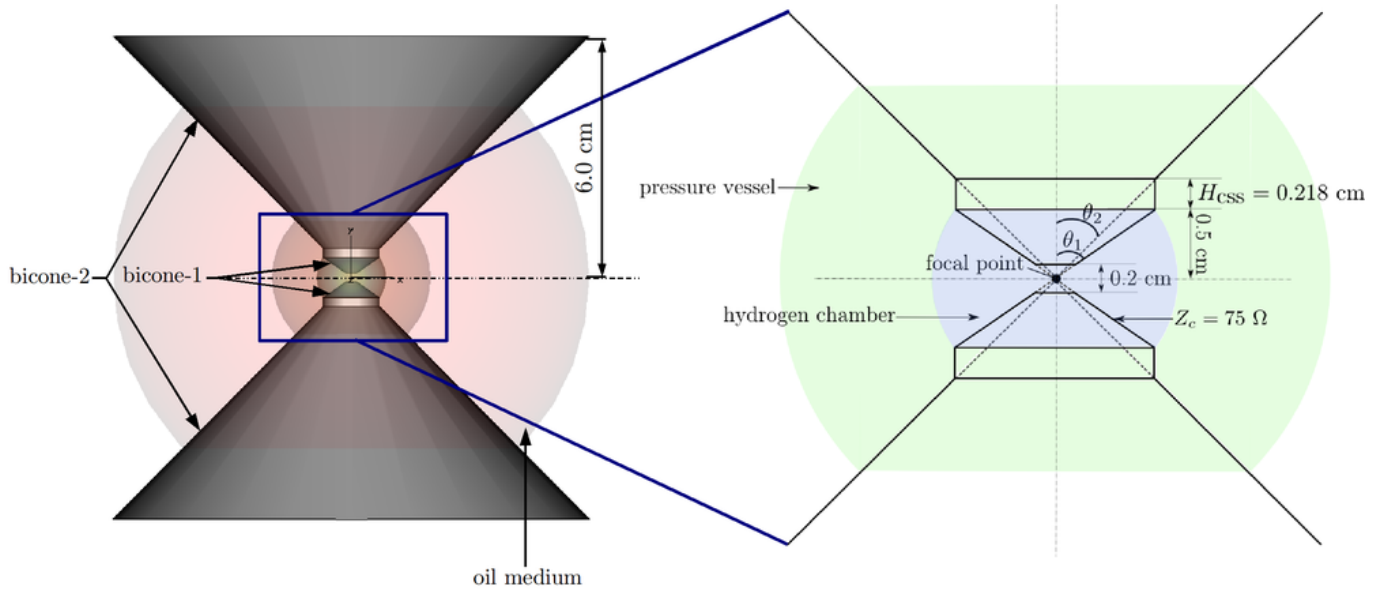


Figure 2.4: Geometrical details and “zoomed-in” side view of switch system for the VBCS-IM-75-SPVSHC configuration.

Geometrical details of bicone-1 and bicone-2 are identical to the VBCS-IM-75-SPVCHC configuration, The dimensions of the switch system components are summarized in Table 2.

Note that the electrical height of the CSS is increased, due to the surrounding pressure vessel medium, by a factor of $\sqrt{\epsilon_{r_{pv}}} = 1.92$ and the electrical height of bicone-2 is increased, due to the surrounding oil medium, by a factor of $\sqrt{\epsilon_{r_{oil}}} = 1.5$.

3 CST parameters

- CST parameters and probe placements are identical to those in [2].

Table 2: Dimensions of switch system components

Component	Height (cm)	Radius (cm)
(mono)cone-1	$h_1 = 0.5$	$r_1 = h_1 \tan \theta_1$
cylindrical support	$H_{\text{css}} = 0.218$	$r_{\text{css}} = h_1 \tan \theta_1$
(mono)cone-2	$h_2 = 6.0$	$r_2 = h_2 \tan \theta_2$
hydrogen chamber	–	$r_{\text{hc}} = h_1 \sec \theta_1$
pressure vessel	–	$r_{\text{pv}} = 2.0$
oil medium	–	$r_{\text{oil}} = 6.0$

- In all simulations, a discrete port, 1 V, 100 ps, ramp rising step, excitation is applied between a 2 mm gap in the switch cones.

Note: Since the input voltage and gap spacing are identical to those in [1], the input power to the 150 Ω VBCS-IM configurations described above is 4/3 (= 200 Ω /150 Ω) times larger than the 200 Ω T4FASC-CSS designs in [1].

4 Results

The time spread in the normalized responses from the near-field electric field probes is summarized in Table 3 (each response is normalized with respect to its maximum).

Table 3: Summary of the approximate time-spread in the normalized near-field electric field responses for the VBCS-IM-75, VBCS-IM-75-SPVCHC and VBCS-IM-75-SPVSHC configurations.

Component	Time spread (ps)	
	VBCS-75-SPVCHC	VBCS-75-SPVCHC
E_ϕ : $-yz$ -plane	0	0
E_θ : $-zx$ -plane	0	0
E_ϕ : xy -plane	≈ 60	≈ 60
E_θ : xy -plane	0	0
E_ϕ : $-zx$ -plane	≈ 5	≈ 5
E_θ : $-yz$ -plane	≈ 60	≈ 60

The results are identical for both configurations. As in [2], the E_ϕ component in the $-yz$ -plane, the E_θ component in the $-zx$ -plane and the E_θ component in the xy -plane are zero. The maximum time spread occurs in the E_ϕ component in the xy -plane and E_θ component in the $-yz$ -plane, ≈ 60 ps. These results lead one to speculate that the geometry of the hydrogen chamber does not significantly affect the electric fields.

The peak focal impulse amplitudes (E_{\max}), spot sizes and Δ FWHMs for both configurations are summarized in Table 4. Δ FWHM is the relative FWHM as defined in [1]. The results are almost identical for both configurations, i.e., the geometry of the hydrogen chamber does not distort the sphericity of the wavefront. E_{\max} is enhanced but is significantly lower than the analogous T4FASC-CSS designs investigated in [1]. The spot diameters and Δ FWHMs are also much larger.

Table 4: Peak focal impulse amplitudes (E_{\max}) and spot sizes for the VBCS-IM-75, VBCS-IM-75-SPVCHC and VBCS-IM-75-SPVSHC configurations.

Configuration	E_{\max} (V/m)	Δ FWHM (ps)	Spot diameter (cm)
VBCS-IM-75-SPVCHC	9.591	21.164	4.542
VBCS-IM-75-SPVSHC	9.394	19.734	4.497

Near-field plots for all configurations are given in Appendix-I. The focal impulse waveforms and the spot sizes are given in Appendix-II.

5 Conclusion

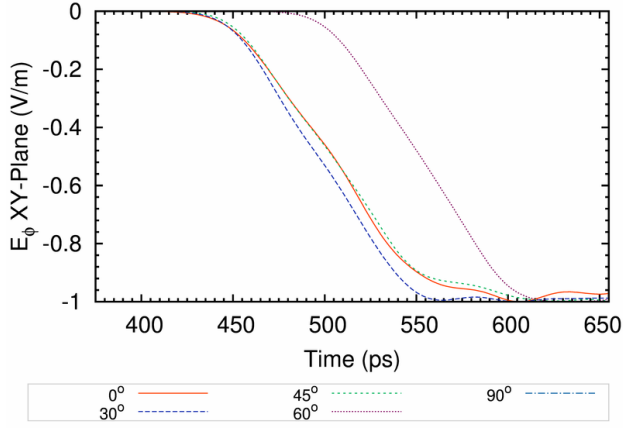
Inspite of the larger input power, the peak focal impulse amplitude for the both the VBCS-IM-75 configurations investigated is significantly lower than the analogous T4FASC-CSS designs in [1]. Therefore, these designs are not attractive for experimental investigation and henceforth will not be considered.

References

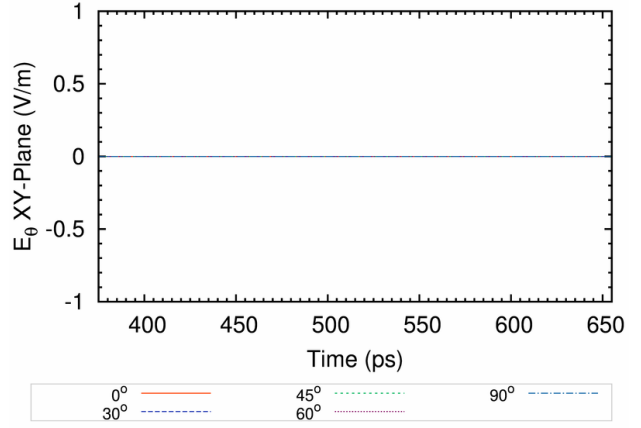
- [1] Prashanth Kumar, Carl E. Baum, Serhat Altunc, Christos G. Christodoulou and Edl Schamiloglu, “The truncated four feed-arm configuration with switch cones (T4FASC) and a spherical pressure vessel.” EM Implosion Memo 42, May 2010.
- [2] Prashanth Kumar, Carl E. Baum, Serhat Altunc, Christos G. Christodoulou and Edl Schamiloglu, “Effect of the impedance of a bicone switch on the focal impulse amplitude and beam width.” EM Implosion Memo 38, Feb. 2010.

APPENDIX-I

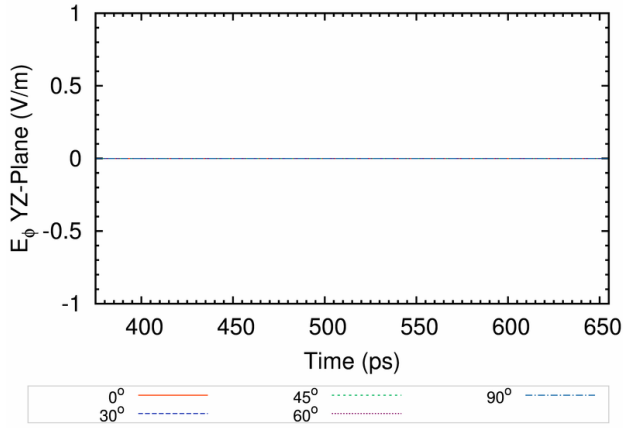
Normalized E_θ and E_ϕ electric field components for the VBCS-IM-75-SPVCHC
and VBCS-IM-75-SPVSHC configurations.



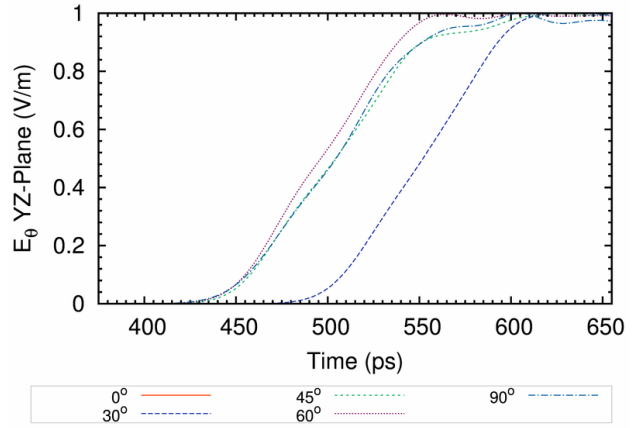
(a) Normalized E_ϕ in the xy -plane



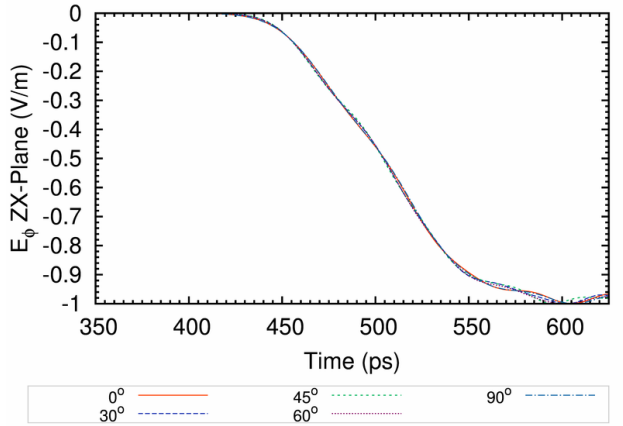
(b) Normalized E_θ in the xy -plane



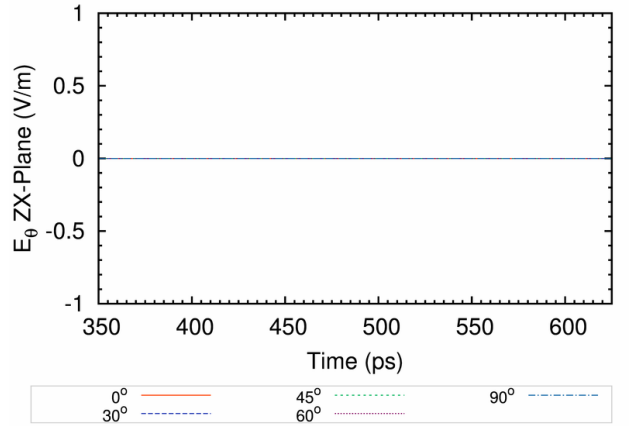
(c) Normalized E_ϕ in the $-yz$ -plane



(d) Normalized E_θ in the $-yz$ -plane

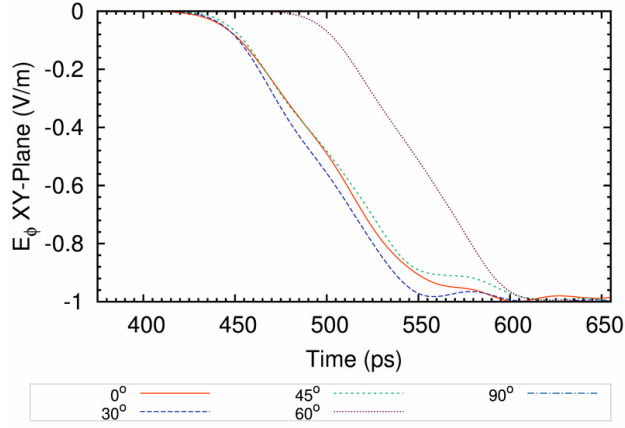


(e) Normalized E_ϕ in the $-zx$ -plane

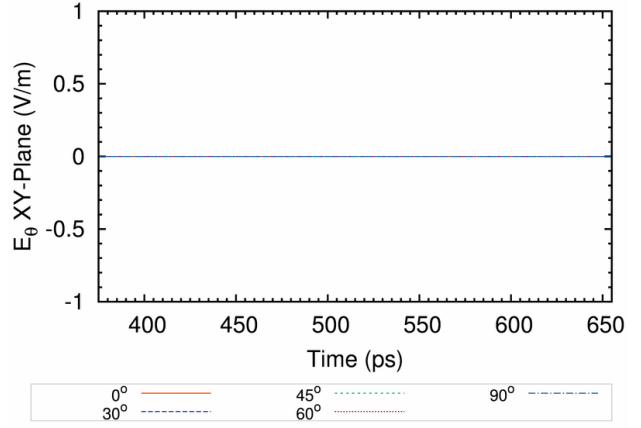


(f) Normalized E_θ in the $-zx$ -plane

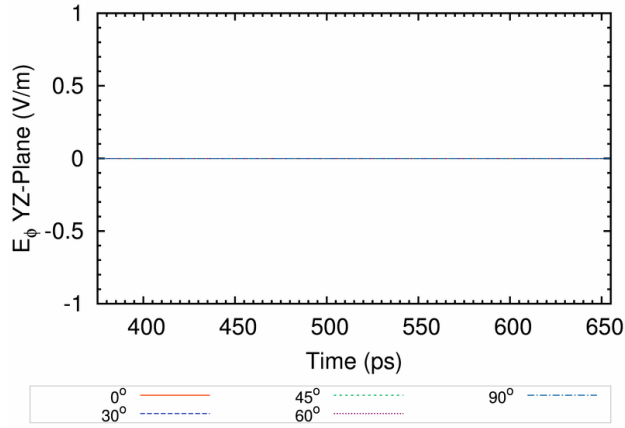
Figure 5.1: Normalized E_θ and E_ϕ components of the responses from the electric field probes on the xy , $-yz$ and $-zx$ planes for the VBCS-IM-75-SPVCHC configuration.



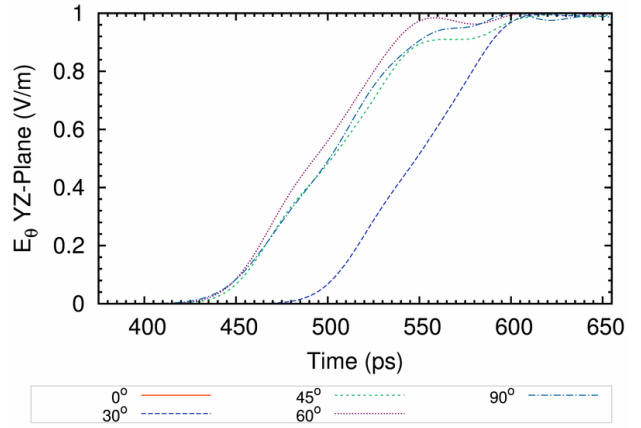
(a) Normalized E_ϕ in the xy -plane



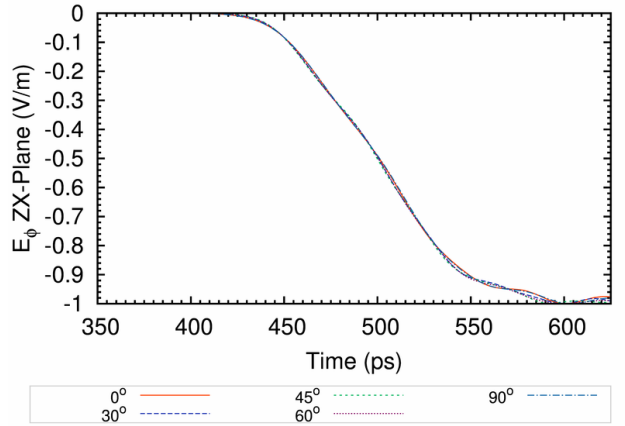
(b) Normalized E_θ in the xy -plane



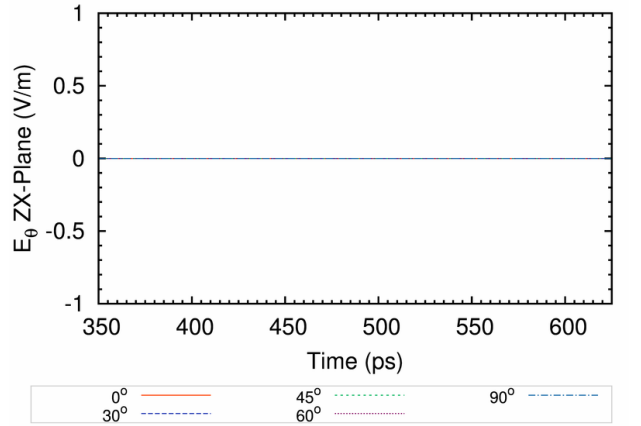
(c) Normalized E_ϕ in the $-yz$ -plane



(d) Normalized E_θ in the $-yz$ -plane



(e) Normalized E_ϕ in the $-zx$ -plane

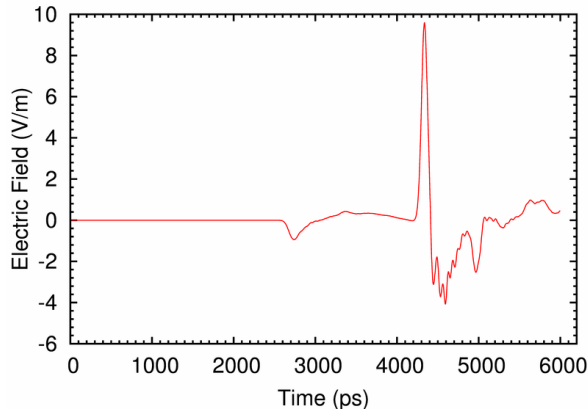


(f) Normalized E_θ in the $-zx$ -plane

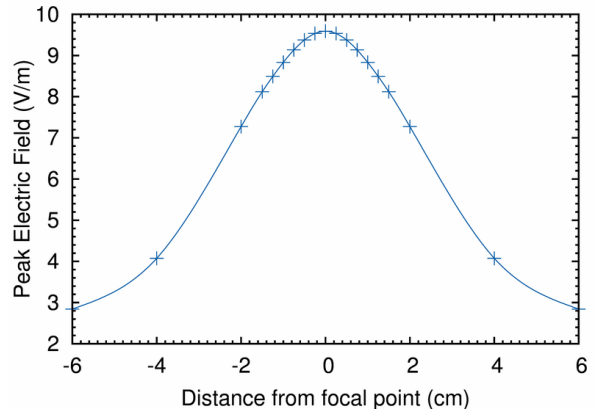
Figure 5.2: Normalized E_θ and E_ϕ components of the responses from the electric field probes on the xy , $-yz$ and $-zx$ planes for the VBCS-IM-75-SPVSHC configuration.

APPENDIX-II

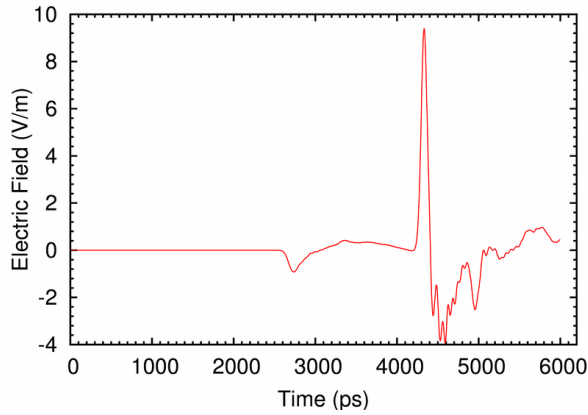
Focal impulse waveforms and beam widths for the VBCS-IM-75-SPVCHC and VBCS-IM-75-SPVSHC configurations.



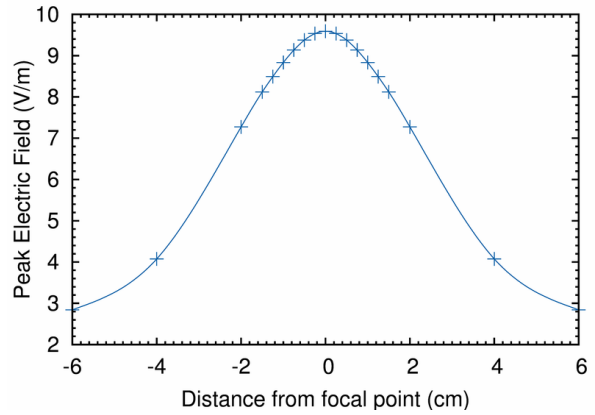
(a) VBCS-IM-75-SPVCHC: Focal impulse waveform.



(b) VBCS-IM-75-SPVCHC: Beam width.



(c) VBCS-IM-75-SPVSHC: Focal impulse waveform.



(d) VBCS-IM-75-SPVSHC: Beam width.

Figure 5.3: Electric field focal impulse waveforms and beam widths for the VBCS-IM-75-SPVCHC and VBCS-IM-75-SPVSHC configurations .